Scripta Materialia 278 (2026) 117284

Contents lists available at ScienceDirect

Scripta Materialia

journal homepage: www.journals.elsevier.com/scripta-materialia

Landau–Lifshitz–Bloch simulations of the magnetocaloric effect in continuous ferromagnetic–paramagnetic transitions

Luis M. Moreno-Ramírez [a,*], Luis Sánchez-Tejerina [a,*], Óscar Alejos [a], Victorino Franco [b], Víctor Raposo [c,d]

[a] Dpto. Electricidad y Electrónica, Universidad de Valladolid 47011 Valladolid, Spain
[b] Multidisciplinary Unit for Energy Science. Dpto. Física de la Materia Condensada, ICMSE-CSIC, Universidad de Sevilla PO Box 1065, 41080-Sevilla, Spain
[c] Dpto. Física Aplicada, Universidad de Salamanca 37008 Salamanca, Spain
[d] Unidad de Excelencia en Luz y Materia Estructuradas (LUMES), Universidad de Salamanca Salamanca, Spain

ARTICLE INFO

Keywords:
Micromagnetic simulations
Landau–Lifshitz–Bloch equation
Magnetocaloric effect and materials
Second-order magnetic transitions

ABSTRACT

The usefulness of modeling magnetocaloric materials expands from the understanding of their behavior to the prediction of new materials, playing a fundamental role in the optimization of their performance. In contrast with other areas of magnetic materials research, micromagnetic simulations of magnetocaloric materials are scarce due to the difficulty of modeling the material in the vicinity of the transition. To solve this limitation, we propose to use the Landau–Lifshitz–Bloch micromagnetic simulations to study the magnetocaloric effect associated with a second-order ferromagnetic↔paramagnetic transition. Following our proposed methodology and considering material parameters in a mean-field framework, we obtain reliable isothermal entropy change curves for monocrystalline and polycrystalline configurations, where we consider different anisotropic contributions. The robustness of the method was evaluated, yielding results that agreed with previous experimental and theoretical observations. Our study shows that micromagnetic simulations are a powerful tool for analyzing second-order magnetocaloric materials with complex microstructures.

The increased energy consumption of cooling systems, combined with existing energy losses, promotes the search for new energy-efficient and green refrigeration technologies [1,2]. In this context, solid-state magnetic refrigeration has been extensively studied in recent decades [3,4]. This technology exploits the magnetocaloric effect (MCE), which is quantified by the reversible adiabatic temperature change or the isothermal entropy change (Δs_{iso}) when a magnetic material is subjected to a variable magnetic field [5]. A deep understanding of the link between performance and material characteristics is key to the design of better magnetocaloric materials (MCMs). This understanding can be achieved through several modeling approaches that focus on different length scales. At one extreme lie atomistic models, which are widely used to obtain different structural and magnetic parameters of materials [6–10], although there are also works to reproduce or predict the MCE [11–16]. Unfortunately, these models are limited to a reduced size of material because of their time-consuming nature. At the other extreme are the macroscopic models based on different thermomagnetic models or equations of state, such as the Landau, Bean-Rodbell or Arrott-Noakes approaches [17–19]. Despite the demonstrated utility of both approaches, they either fail to describe or overly simplify various relevant characteristics of real samples, such as magnetic domains or granular structure, that nonetheless can have a substantial impact on the MCE [20–24]. Neglecting such characteristics in the models has two deleterious effects: on the one hand, if material optimization significantly relies on microstructural engineering, their influence cannot be adequately described. On the other hand, data analysis is also affected by these simplifications, in particular the field dependence of Δs_{iso} [25–29].

Microscopic models appear to be an optimal alternative between these two extreme approaches, as they allow magnetic materials with complex microstructures to be replicated [30,31]. However, there have been limited attempts for MCMs mainly due to the limitations of de-

* Corresponding authors.
E-mail addresses: luis.moreno.ramirez@uva.es (L.M. Moreno-Ramírez), luis.sanchez-tejerina@uva.es (L. Sánchez-Tejerina).

https://doi.org/10.1016/j.scriptamat.2026.117284
Received 26 November 2025; Received in revised form 17 February 2026; Accepted 14 March 2026
Available online 19 March 2026
1359-6462/© 2026 The Author(s). Published by Elsevier Inc. on behalf of Acta Materialia Inc. This is an open access article under the CC BY-NC-ND license (http://creativecommons.org/licenses/by-nc-nd/4.0/).

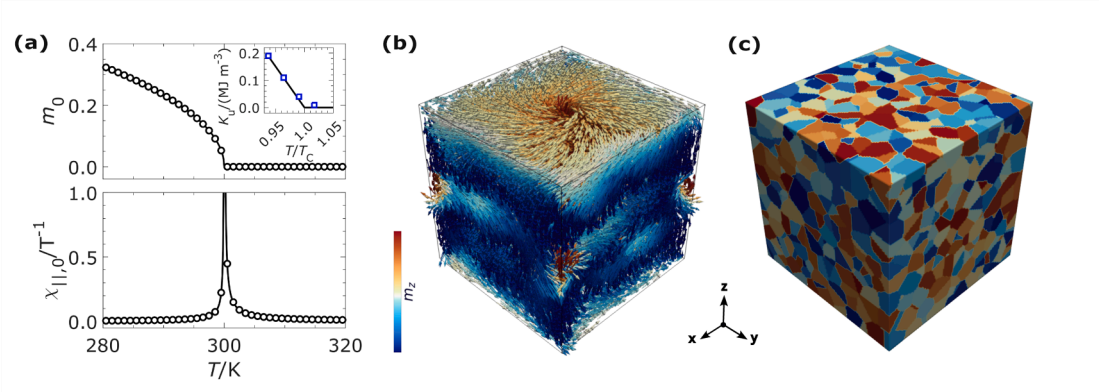

Fig. 1. (a) Temperature dependence of the LLB inputs: magnitude of the zero-field reduced magnetization (up) and zero-field reduced longitudinal susceptibility (down). Inset: Temperature-dependent uniaxial anisotropy constant, square symbols for experimental data [41]. (b) Equilibrium magnetization at 280 K and 0.001 T for a monocrystal composed of $128 \times 128 \times 128$ cells. (c) Polycrystalline sample with microstructure generated by Voronoi tessellation (each grain region is colored to distinguish it).

scribing the material around its transition temperature. In this sense, the work in [32] stands out, where micromagnetic modeling based on the Landau-Lifshitz-Gilbert equation was employed in the ferromagnetic (FM) range up to temperatures close (but below) the Curie temperature (T_C). However, the behavior for higher temperatures, including the paramagnetic (PM) range, was extrapolated by fitting previous micromagnetic results in the FM range to the Arrott-Noakes equation of state. Alternatively, we propose the study of the MCE of a ferromagnetic material undergoing a second-order FM↔PM transition employing micromagnetic simulations based on the Landau-Lifshitz-Bloch (LLB) equation [33,34] in the whole temperature range. This equation has turned out to be highly useful in various contexts close to the critical temperature, such as heat assisted magnetic recording [35–37], ultrafast dynamics induced by laser excitation [38,39], or domain wall motion in thermal gradients [40]. Using LLB micromagnetic simulations, we reproduced the MCE for monocrystalline and polycrystalline materials and evaluated the influence of sample geometry, magnetocrystalline anisotropy, and microstructure on Δs_{iso}. Additionally, we paid special attention to the field dependence analysis, i.e., universal curve and exponent n.

To perform this study, we implemented the classical LLB equation into a customized micromagnetic software based on MuMax^3 [40,42] to obtain the total equilibrium magnetization ($\boldsymbol{M}$) of a ferromagnetic material around its T_C for different applied fields ($\boldsymbol{H}$). Further details of the micromagnetic LLB simulations are included in the supplementary material. Temperature-dependent material inputs for the simulations for each micromagnetic cell such as the magnitude of the reduced magnetization at zero applied field (m_0) and the longitudinal reduced magnetic susceptibility for zero applied field ($\chi_{\parallel,0}$) need to be introduced. We employed the mean-field-based Brillouin theory in the classical limit for both inputs [43]:

$$m_0 = \mathcal{L}(x)\,, \tag{1}$$

$$\chi_{\parallel,0} = \frac{\mu \mathcal{L}'(x)}{k_B T\left(1 - 3T_C \mathcal{L}'(x)/T\right)}\,, \tag{2}$$

where $\mathcal{L}$ and $\mathcal{L}'$ are the Langevin function and its derivative, respectively, $x = 3m_0 T_C/T$, μ the atomic magnetic moment, and k_B the Boltzmann constant. The inputs with chosen material parameters (described in this section) are depicted in Fig. 1(a). The Brillouin theory ensures the critical behavior of the magnetization near the transition being characterized by the mean-field critical exponents $\beta = 0.5$ and $\delta = 3$. In addition, it yields the critical scaling for Δs_{iso} and reproduces the characteristic value of 2/3 for the exponent n at T_C [26]. Other inputs based on different macroscopic model, measurement, or ab-initio calculation can also be used without compromising the validity of our approach. It must be emphasized that the present study is restricted to second-order MCMs without magnetoelastic contribution. Accordingly, owing to the intrinsic characteristics of second-order transitions, neither thermal/magnetic hysteresis associated to the transition nor phase coexistence is considered. For the simulations, cubic micromagnetic cells with 4 nm edges were used for different sample geometries. This cell size is smaller than the exchange length ensuring the continuum approximation is valid and properly characterizes the changes in magnetization according to the parameters of the selected material. Additionally, this size is large enough to limit the thermal fluctuations for the explored temperature range. As an example, the equilibrium magnetization solution for $128 \times 128 \times 128$ cells is shown in Fig. 1(b). We considered material parameters similar to those of the $AlFe_2B_2$ alloy, an interesting rare-earth-free second-order MCM for room temperature applications [44–47]. Thus, $\mu = 1\,\mu_B$, $T_C = 300$ K, saturation magnetization (M_{sat}) of 407 kA m^{-1} (80 A m^2 kg^{-1}), and exchange stiffness at 0 K (A_0) of 1.4 pJ m^{-1}. Given the narrow temperature span examined in this study and the good reproducibility of the experimental data [41], we considered a uniaxial magnetocrystalline anisotropy in which the first-order anisotropy constant (K_u) decreases linearly with temperature and vanishes at T_C (inset of Fig. 1(a)). It should be emphasized that alternative methods, including the standard Callen-Callen scaling law as well as experimental or ab-initio based data sets [48–52], can be straightforwardly incorporated into our approach. The different granular microstructures of the polycrystalline samples were generated by the Voronoi tessellation method implemented in MuMax^3 [53] (an example is shown in Fig. 1(c)).

To evaluate the MCE, Δs_{iso} is calculated from the total magnetization through the Maxwell relations following a discrete approximation to:

$$\Delta s_{iso} = \mu_0 \int_{\mathbf{0}}^{\boldsymbol{H_f}} \left(\frac{\partial \boldsymbol{M}}{\partial T}\right)_{\boldsymbol{H}} \cdot \mathrm{d}\boldsymbol{H}, \tag{3}$$

where $\boldsymbol{H_f}$ is the final applied magnetic field [54]. The scaling behavior of Δs_{iso} is tested by the phenomenological universal curve [25,26]. This curve is constructed by rescaling both Δs_{iso} and temperature axis for different magnetic field changes. First, Δs_{iso} is normalized by its peak value for each field (Δs_{iso}^{pk}). Second, for rescaling the temperature axis, the reference temperatures (T_r) are defined as the temperature for which the normalized value of Δs_{iso} is the same in both FM and PM ranges (0.7 in this study). Once T_r is obtained for each field, the temperature axis is rescaled as $(T - T_{pk})/(T_r - T_{pk})$ where T_{pk} is the peak temperature. The field dependence exponent n is calculated following a discrete approximation to:

$$n = \frac{\partial \ln(|\Delta s_{iso}|/|\Delta s_{iso}(1\,\mathrm{T})|)}{\partial \ln(\Delta H/(1\,\mathrm{T}))}, \tag{4}$$

where ΔH is the magnitude of the applied magnetic field change.

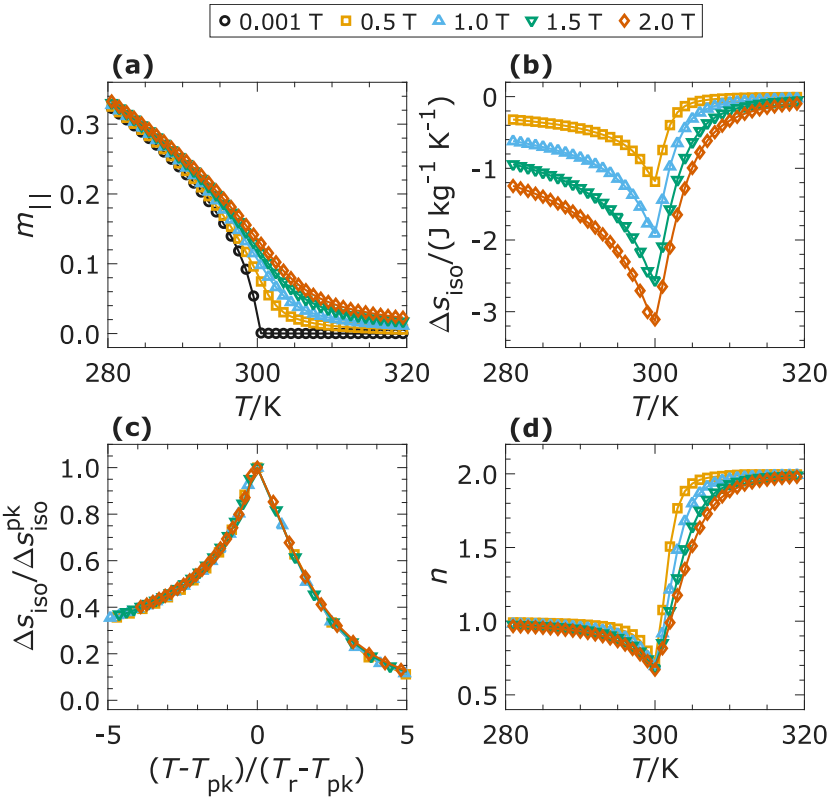

Fig. 2. Temperature dependence of the (a) longitudinal reduced magnetization, (b) isothermal entropy change, (c) phenomenological universal curve, and (c) exponent n for different applied fields and field changes. The hollow symbols correspond to the micromagnetic results, while the solid lines corresponds to the Brillouin solutions.

The simulations were conducted using external conditions similar to the experimental ones to calculate (3) and (4). A temperature step of 1 K around T_C is selected. For the magnetic field, we simulated up to 40 fields from 0.001 T to 2 T following a quadratic progression. First, we simulated a monocrystalline material without anisotropy, thus, resulting in a homogeneously magnetized material. Therefore, the simulation results can be compared with those from macroscopic models with single-domain magnetization. For this comparison, we selected the Brillouin theory in the classical limit to ensure consistency with the inputs used and because it has proven highly useful in the modeling of MCMs [55]. The simulation results are depicted as hollow symbols in Fig. 2, while the corresponding results of the Brillouin theory are plotted as solid lines. An excellent agreement was observed between them for all the physical quantities explored even for 2 T. For the longitudinal reduced magnetization ($m_{||}$), the deviations with respect to the Brillouin theory are below 0.1 % in the temperature and field ranges explored (Fig. 2(a)). For Δs_{iso}, the deviations are found to be below 1.9 %, being more significant around T_C and for the largest applied field changes (Fig. 2(b)). These minor deviations have a negligible influence on subsequent field dependence analysis, as can be observed from the excellent collapse of the universal construction (Fig. 2(c)). The exponent n showed the expected behavior for a mean-field Curie transition: 1 for $T << T_C$, 2 for $T >> T_C$, and 2/3 at T_C (Fig. 2(d)). From the simulations $n(T_C) = 0.696$, which deviates a 4.5 % from the theoretical value. This deviation is moderate considering that to calculate the exponent n: 1) the initial magnetization data is derived twice and 2) a discrete approach is followed. Similar deviations are found for the Brillouin calculations under the same conditions. These findings demonstrate that the simulations successfully replicate the MCE. From now on, the comparison with Brillouin theory cannot be established as we will incorporate different energy density contributions that lead to non-uniform magnetization.

We next examined the effect of the demagnetizing field on the MCE. For that, we simulated a monocrystalline material with different sample geometries and field orientations. The micromagnetic solver allows the introduction of the demagnetizing field by using a discrete convolution of the magnetization with a demagnetizing kernel [42], allowing the calculation of the demagnetizing field even for non-uniform magnetization states. However, we calculated the corresponding effective demagnetizing factor (N) associated with the relevant axis for each case in the uniform state, using it solely as a label for the corresponding case. The values of N corresponding to each geometry are tabulated in the supplementary material. As an example of a given geometry, the magnetization data for low applied fields for a cubic sample composed of $128 \times 128 \times 128$ cells (label $N = 0.33$) are shown in Fig. 3(a). The demagnetizing field reduces the total magnetization of the sample in the FM range compared to the uniform state. This effect is overcome for applied fields slightly above the demagnetizing one (~ 55 mT at 280 K. Next, for $N = 0, 0.33$ and 0.77 cases, Δs_{iso}, universal construction, and exponent n are shown in panels (b), (c), and (d) of Fig. 3, respectively. Δs_{iso} is reduced by the effect of the demagnetizing field, showing an almost constant reduction in the FM range that vanishes slightly above T_C. In addition, the larger the demagnetizing factor, the larger the deviations. These deviations saturate for fields slightly above the demagnetizing field, becoming almost field independent after that (e.g. achieving a reduction of 0.07 J kg^{-1} K^{-1} for the $N = 0.77$ case at 280 K). For fields of technological interest, such as 1 T, its relative effect is moderate around the peak (e.g., deviations of about −3 % for the $N = 0.77$ case). In addition, they degrade the universal collapse for low applied field changes and low temperatures, although its effect is negligible for fields clearly above the demagnetizing one. Finally, the demagnetizing field significantly overestimates the exponent n for $T \leq T_C$ (achieving deviations of about 100 % for low fields). Similarly to the previous results, the deviations increase as the demagnetizing factor increases and the temperature

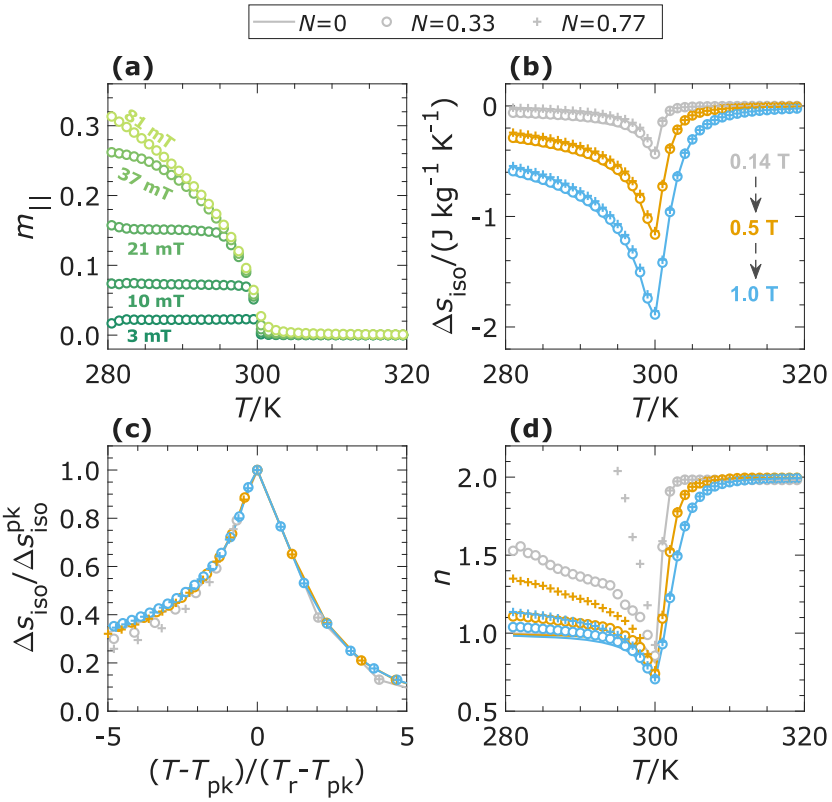

Fig. 3. (a) Temperature dependence of the longitudinal reduced magnetization for low applied fields for a sample with cubic geometry. Temperature dependence of the (b) isothermal entropy change, (c) phenomenological universal curve, and (d) exponent *n* for different samples and orientations with corresponding demagnetizing factor label.

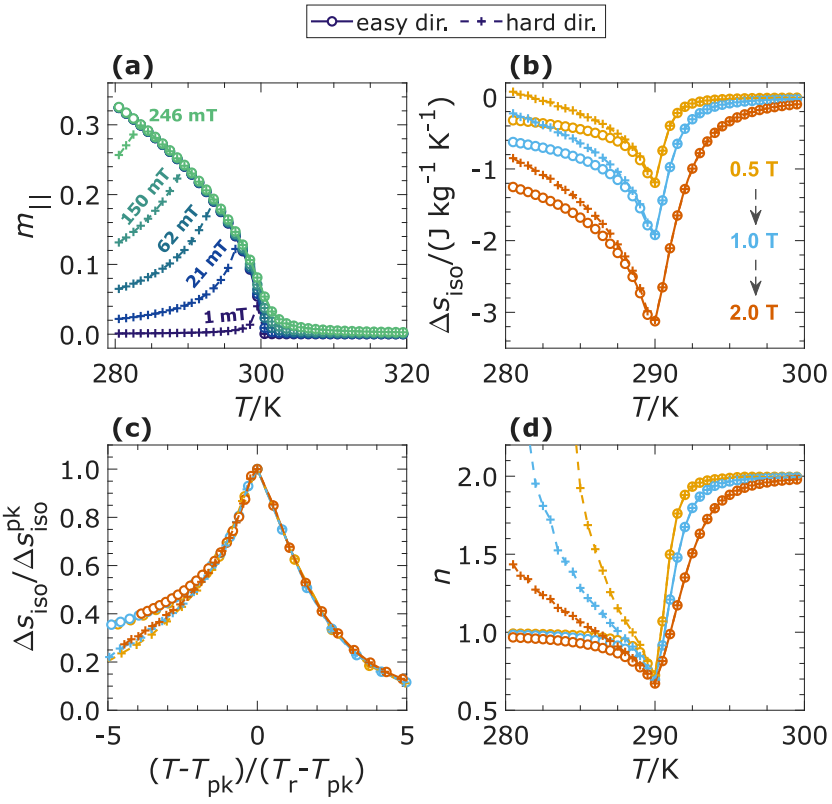

Fig. 4. (a) Temperature dependence of the longitudinal magnetization for low applied fields along easy and hard directions. Calculated (b) isothermal entropy change, (c) phenomenological construction, and (d) exponent *n* for different applied field changes along easy and hard axis.

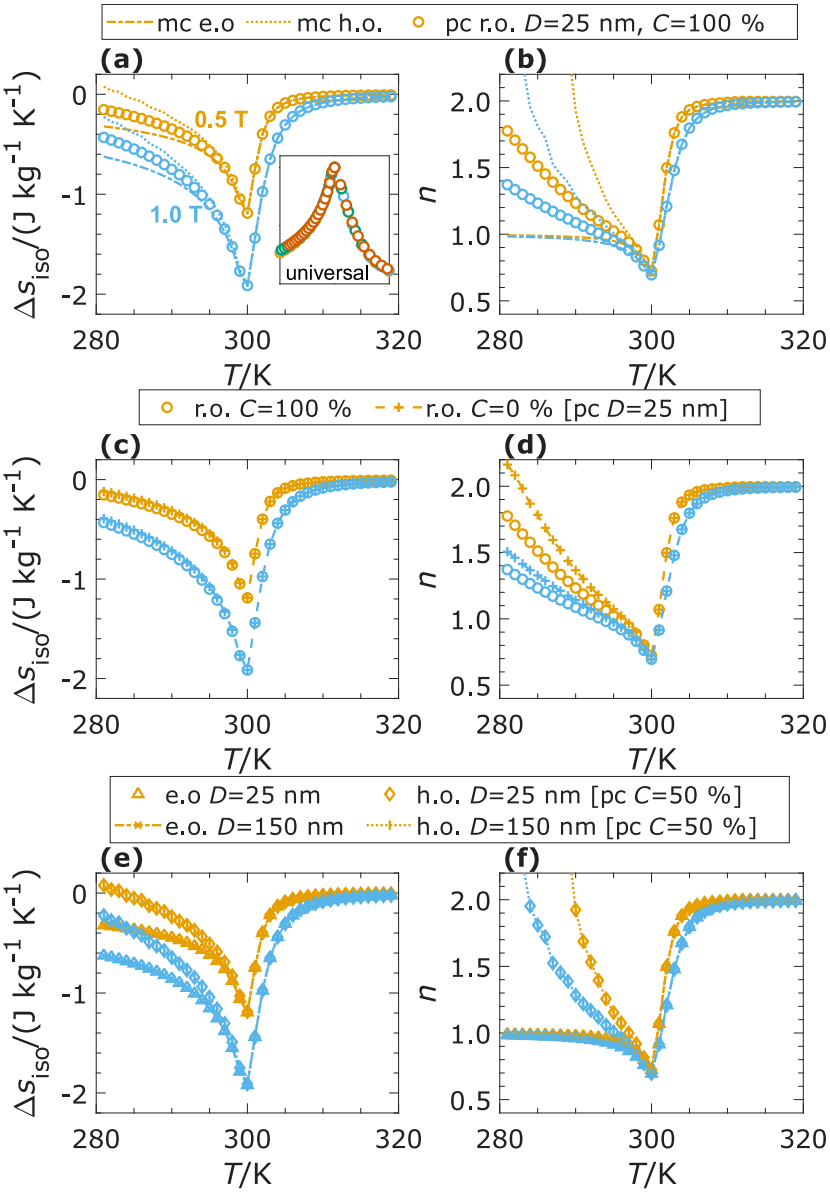

Fig. 5. Isothermal entropy change (left) and exponent n (right) for: 1) polycrystal (pc) with randomly orientated grains and monocrystal (mc) for both easy (e.o.) and hard (h.o.) orientations [(a) and (b)], 2) polycrystal with randomly orientated grains with different exchange coupling between grains, C [(c) and (d)] and 3) oriented polycrystal with different mean grain size, D [(e) and (f)]. Corresponding phenomenological construction of panel (a) data is shown in as an inset (same scale and units as previous plots).

decreases. The magnetic field change strength tends to diminish the deviations, although their effects are still notable even for 1 T (e.g. $\sim 14\,\%$ for the $N = 0.77$ case at 280 K). There is also a significant effect at T_C characterized by a linearly increasing relationship between $n(T_C)$ and N (see Figure S.2.1 of the supplementary material). These deviations from the expected theoretical values (e.g $\sim 5\,\%$ for the $N = 0.77$ case) can lead to erroneous interpretations of the critical exponents. These conclusions agree with previous theoretical and experimental results [56–58], which highlight the importance of reducing the demagnetizing fields to obtain an accurate physical interpretation.

In the following, we included the magnetocrystalline anisotropy as previously described. A thin square sheet of $512 \times 512 \times 8$ cells with an in-plane uniaxial anisotropy axis is chosen to avoid additional demagnetizing effects, as both easy and hard orientations lie in the sample plane. The physical quantities explored are shown in Fig. 4. The magnetization along the easy orientation coincides with the total magnetization magnitude, whereas the values for the hard orientation are considerably reduced for low fields (Fig. 4(a)). They show an increasing trend with temperature until the anisotropy field is overcome. After that, the magnetization is the same for both easy and hard axes. The larger the applied field, the lower the temperature required to saturate the magnetization. For Δs_{iso} two differentiated responses in the FM range are observed according to the applied field orientation, being smaller for the hard orientation than for the easy one (Fig. 4(b)). These differences decrease as the temperature increases, vanishing at T_C. For the universal construction, two different curves associated with each applied field orientation are observed (Fig. 4(c)). This behavior is found experimentally, as shown in [59]. For the exponent n, applying the field along the hard axis causes strong deviations in the FM range from the theoretical value of 1 (about $\sim 100\,\%$), similar to the effects of shape anisotropy but without influence at $T = T_C$ (Fig. 4(d)). Alternatively, this anisotropic MCE can be exploited in devices with rotating fields [16,60]. Our ap-

proach also accounts for this behavior as shown in the supplementary material.

Finally, granular microstructures with different crystalline orientation distributions were explored. A thin square sheet is used to avoid additional in-plane demagnetizing effects. The MCE is simulated for a randomly oriented polycrystal with a mean grain size (D) of 25 nm and 100 % exchange coupled grains ($C = 100\,\%$). Δs_{iso} and exponent n are depicted in panels (a) and (b) of Fig. 5, respectively, together with the previously characterized monocrystal response. As experimentally observed for randomly oriented grains, the polycrystal response for both Δs_{iso} and exponent n is the average of the easy and hard responses of the monocrystal [61]. The universal construction is depicted in the inset of panel (a) (same representation range as before). An excellent collapse is observed, which is an interesting result despite the double universal curve observed for the uniaxial monocrystal (see Fig. 4(c)). This demonstrates the robustness of the phenomenological construction for polycrystalline samples. We have also analyzed the influence of exchange coupling between grains by reducing it from fully coupled to decoupled, as shown in panels (c) and (d) of Fig. 5. Decoupling the grains causes a slight reduction in Δs_{iso} (e.g. a reduction about 10 % for 1 T and 280 K) that vanishes at T_C. However, its effect on the exponent n is more significant, increasing the values in the FM range ($\sim 40\,\%$). These deviations decrease with increasing temperature, vanishing at T_C. The lower the field change, the larger the effect. Notably, with this grain boundary modeling, we avoid the addition of secondary material, which also tends to diminish the total effect per mass (or per volume) and hide the real grain boundary influence. Finally, we decided to align all the grains along the same orientation to check the influence of the mean grain size without the undesired effect of not fully random distributed orientations in the case of large grains. The responses for grain-oriented distributions with 25 nm and 150 nm mean sizes are illustrated in panels (e) and (f) of Fig. 5, respectively. No significant differences were observed for either the orientation or applied field changes. These results indicate that grain size effects are negligible, while grain boundary effects are minimal for Δs_{iso} but significant for exponent n.

To conclude, we have shown that using micromagnetic simulations based on the LLB equation, we were able to reproduce the MCE associated with a second-order FM ↔ PM transition. Using parameters similar to those of $AlFe_2B_2$, a rare-earth-free magnet with notable room-temperature response, we calculated the magnetocaloric response in monocrystal and polycrystal configurations. This latter case exemplifies the virtues of our proposed methodology, being challenging to analyze through macroscopic or atomic approaches. The effect of the shape and magnetocrystalline anisotropy on Δs_{iso} is analyzed, paying special attention to the field-dependence behavior through the universal curve and exponent n. The results obtained are in agreement with previous experimental or theoretical approaches, demonstrating the capability of micromagnetic simulations to characterize second-order MCMs with complex microstructures. We expect that this work provides an opportunity to further extend the presented approach towards the description of first-order MCMs by including magnetoelastic and kinetical effects.

CRediT authorship contribution statement

Luis M. Moreno-Ramírez: Writing – review & editing, Writing – original draft, Visualization, Validation, Methodology, Investigation, Formal analysis, Data curation, Conceptualization; **Luis Sánchez-Tejerina:** Writing – review & editing, Writing – original draft, Validation, Software, Methodology, Investigation, Formal analysis, Conceptualization; **Óscar Alejos:** Writing – review & editing, Validation, Resources, Investigation, Conceptualization; **Victorino Franco:** Writing – review & editing, Validation, Funding acquisition, Conceptualization; **Víctor Raposo:** Writing – review & editing, Validation, Software, Funding acquisition, Conceptualization.

Declaration of competing interest

The authors declare that they have no known competing financial interests or personal relationships that could have appeared to influence the work reported in this paper.

Acknowledgments

We acknowledge funding from Projects PID2023-150853NB-C31 and PID2023-146047OBI00 funded by MICIU/AEI/10.13039/501100011033 and FEDER, and project Magccine funded by the European Union and the European Innovation Council.

Supplementary material

Supplementary material associated with this article can be found in the online version at 10.1016/j.scriptamat.2026.117284.

References

[1] S. Pezzutto, G. Quaglini, P. Riviere, L. Kranzl, A. Novelli, A. Zambito, E. Wilczynski, Screening of cooling technologies in Europe: alternatives to vapour compression and possible market developments, Sustainability 14 (2022). https://doi.org/10.3390/su14052971

[2] Eurostat, Shedding Light on Energy in Europe - 2025 Edition, Technical Report, European Union, 2025. https://doi.org/10.2785/8045944

[3] V. Franco, J.S. Blázquez, J.J. Ipus, J.Y. Law, L.M. Moreno-Ramírez, A. Conde, Magnetocaloric effect: from materials research to refrigeration devices, Prog. Mater. Sci. 93 (2018) 112–232. https://doi.org/10.1016/j.pmatsci.2017.10.005

[4] A. Kitanovski, Energy applications of magnetocaloric materials, Adv. Energy Mater. 10 (2020) 1903741. https://doi.org/10.1002/aenm.201903741

[5] P. Weiss, A. Piccard, Le phénomène magnétocalorique, J. de Physique Théorique et Appliquée 7 (1917) 103–109. https://doi.org/10.1051/jphystap:019170070010300

[6] D. Paudyal, V.K. Pecharsky, K.A. Gschneidner, B.N. Harmon, Electron correlation effects on the magnetostructural transition and magnetocaloric effect in $Gd_5Si_2Ge_2$, Phys. Rev. B 73 (2006) 144406. https://doi.org/10.1103/PhysRevB.73.144406

[7] Z. Gercsi, K. Hono, K.G. Sandeman, Designed metamagnetism in $CoMnGe_{1-x}P_x$, Phys. Rev. B - Condens. Matter Mater. Phys. 83 (2011) 174403. https://doi.org/10.1103/PhysRevB.83.174403

[8] F. Guillou, A.K. Pathak, D. Paudyal, Y. Mudryk, F. Wilhelm, A. Rogalev, V.K. Pecharsky, Non-hysteretic first-order phase transition with large latent heat and giant low-field magnetocaloric effect, Nat. Commun. 9 (2018) 2925. https://doi.org/10.1038/s41467-018-05268-4

[9] L.M. Moreno-Ramírez, C. Romero-Muñiz, J.Y. Law, V. Franco, A. Conde, I.A. Radulov, F. Maccari, K.P. Skokov, O. Gutfleisch, Tunable first order transition in $La(Fe,Cr,Si)_{13}$ compounds: retaining magnetocaloric response despite a magnetic moment reduction, Acta Mater. 175 (2019) 406–414. https://doi.org/10.1016/j.actamat.2019.06.022

[10] A. Biswas, A.K. Pathak, N.A. Zarkevich, X. Liu, Y. Mudryk, V. Balema, D.D. Johnson, V.K. Pecharsky, Designed materials with the giant magnetocaloric effect near room temperature, Acta Mater. 180 (2019) 341–348. https://doi.org/10.1016/j.actamat.2019.09.023

[11] E.P. Nóbrega, N.A. de Oliveira, P.J. von Ranke, A. Troper, Monte Carlo calculations of the magnetocaloric effect in $Gd_5(Si_xGe_{1-x})_4$ compounds, Phys. Rev. B 72 (2005) 134426. https://doi.org/10.1103/PhysRevB.72.134426

[12] J.B. Staunton, A. Marmodoro, A. Ernst, Using density functional theory to describe slowly varying fluctuations at finite temperatures: local magnetic moments in Gd and the 'not so local' moments of Ni, J. Phys.: Condens. Matter 26 (2014) 274210. https://doi.org/10.1088/0953-8984/26/27/274210

[13] D. Comtesse, M.E. Gruner, M. Ogura, V.V. Sokolovskiy, V.D. Buchelnikov, A. Grünebohm, R. Arróyave, N. Singh, T. Gottschall, O. Gutfleisch, V.A. Chernenko, F. Albertini, S. Fähler, P. Entel, First-principles calculation of the instability leading to giant inverse magnetocaloric effects, Phys. Rev. B 89 (2014) 184403. https://doi.org/10.1103/PhysRevB.89.184403

[14] J.D. Bocarsly, E.E. Levin, C.A.C. Garcia, K. Schwennicke, S.D. Wilson, R. Seshadri, A simple computational proxy for screening magnetocaloric compounds, Chem. Mater. 29 (2017) 1613–1622. https://doi.org/10.1021/acs.chemmater.6b04729

[15] C. Romero-Muñiz, J.Y. Law, L.M. Moreno-Ramírez, Á. Díaz-García, V. Franco, Using a computationally driven screening to enhance magnetocaloric effect of metal monoborides, J. Phys. Energy 5 (2023) 024021. https://doi.org/10.1088/2515-7655/acce6e

[16] R. Almeida, S.C. Freitas, C.R. Fernandes, R. Kiefe, J.P. Araújo, J.S. Amaral, J.O. Ventura, J.H. Belo, D.J. Silva, Rotating magnetocaloric effect in polycrystals-harnessing the demagnetizing effect, J. Phys. Energy 6 (2024) 015020. https://doi.org/10.1088/2515-7655/ad1c61

[17] A. Arrott, J.E. Noakes, Approximate equation of state for nickel near its critical temperature, Phys. Rev. Lett. 19 (1967) 786–789. https://doi.org/10.1103/PhysRevLett.19.786

[18] C.P. Bean, D.S. Rodbell, Magnetic disorder as a first-order phase transformation, Phys. Rev. 126 (1962) 104–115. https://doi.org/10.1103/PhysRev.126.104

[19] M.D. Kuz'min, Landau-type parametrization of the equation of state of a ferromagnet, Phys. Rev. B 77 (2008) 184431. https://doi.org/10.1103/PhysRevB.77.184431

[20] T. Gottschall, D. Benke, M. Fries, A. Taubel, I.A. Radulov, K.P. Skokov, O. Gutfleisch, A matter of size and stress: understanding the first-order transition in materials for solid-state refrigeration, Adv. Funct. Mater. 27 (2017) 1606735. https://doi.org/10.1002/adfm.201606735

[21] J. Lai, H. Sepehri-Amin, X. Tang, J. Li, Y. Matsushita, T. Ohkubo, A.T. Saito, K. Hono, Reduction of hysteresis in $(La_{1-x}Ce_x)_y(Mn_zFe_{11.4-z})Si_{1.6}$ magnetocaloric compounds for cryogenic magnetic refrigeration, Acta Mater. 220 (2021) 117286. https://doi.org/10.1016/j.actamat.2021.117286

[22] F. Zhang, Z. Wu, J. Wang, W. Chen, Z. Wu, X. Chi, C. Zhao, S. Eijt, H. Schut, X. Bai, Y. Ren, N. van Dijk, E. Brück, Impact of fast-solidification on all-d-metal NiCoMnTi based giant magnetocaloric Heusler compounds, Acta Mater. 265 (2024) 119595. https://doi.org/10.1016/j.actamat.2023.119595

[23] Á. Díaz-García, J.Y. Law, L.M. Moreno-Ramírez, V. Franco, Stress-relieved Fe – Mn – Ni – Ge – Si high-entropy alloys: a path for enhancing the magnetocaloric response, Scr. Mater. 258 (2025) 116492. https://doi.org/10.1016/j.scriptamat.2024.116492

[24] M.M. Prusty, S.H. Molleti, T. Hiroto, S.R.K. Malladi, X. Tang, H. Sepehri-Amin, Reduced hysteresis in $La_{0.7}Ce_{0.3}Fe_{11.5}Si_{1.5}$ hydrides by grain size reduction, Sci. Technol. Adv. Mater. (2025) 2525742. https://doi.org/10.1080/14686996.2025.2525742

[25] V. Franco, A. Conde, J.M. Romero-Enrique, J.S. Blázquez, A universal curve for the magnetocaloric effect: an analysis based on scaling relations, J. Phys.: Condens. Matter 20 (2008) 285207. https://doi.org/10.1088/0953-8984/20/28/285207

[26] V. Franco, A. Conde, Scaling laws for the magnetocaloric effect in second order phase transitions: from physics to applications for the characterization of materials, Int. J. Refrig. 33 (2010) 465–473. https://doi.org/10.1016/j.ijrefrig.2009.12.019

[27] C.M. Bonilla, J. Herrero-Albillos, F. Bartolomé, L.M. García, M. Parra-Borderías, V. Franco, Universal behavior for magnetic entropy change in magnetocaloric materials: an analysis on the nature of phase transitions, Phys. Rev. B - Condens. Matter Mater. Phys. 81 (2010) 224424. https://doi.org/10.1103/PhysRevB.81.224424

[28] V. Franco, J.Y. Law, A. Conde, V. Brabander, D.Y. Karpenkov, I. Radulov, K. Skokov, O. Gutfleisch, Predicting the tricritical point composition of a series of LaFeSi magnetocaloric alloys via universal scaling, J. Phys. D Appl. Phys. 50 (2017) 414004. https://doi.org/10.1088/1361-6463/aa8792

[29] J.Y. Law, V. Franco, L.M. Moreno-Ramírez, A. Conde, D.Y. Karpenkov, I. Radulov, K.P. Skokov, O. Gutfleisch, A quantitative criterion for determining the order of magnetic phase transitions using the magnetocaloric effect, Nat. Commun. 9 (2018) 2680. https://doi.org/10.1038/s41467-018-05111-w

[30] T. Schrefl, J. Fidler, H. Kronmüller, Remanence and coercivity in isotropic nanocrystalline permanent magnets, Phys. Rev. B 49 (1994) 6100–6110. https://doi.org/10.1103/PhysRevB.49.6100

[31] H. Sepehri-Amin, T. Ohkubo, S. Nagashima, M. Yano, T. Shoji, A. Kato, T. Schrefl, K. Hono, High-coercivity ultrafine-grained anisotropic Nd-Fe-B magnets processed by hot deformation and the Nd-Cu grain boundary diffusion process, Acta Mater. 61 (2013) 6622–6634. https://doi.org/10.1016/j.actamat.2013.07.049

[32] D. Ohmer, M. Yi, M. Fries, O. Gutfleisch, B.-X. Xu, Calculating the magnetocaloric effect in second-order-type material by micromagnetic simulations: a case study on Co_2B, Scr. Mater. 177 (2020) 218–222. https://doi.org/10.1016/j.scriptamat.2019.10.039

[33] D.A. Garanin, V.V. Ishchenko, L.V. Panina, Dynamics of an ensemble of single-domain magnetic particles, Theor. Math. Phys. 82 (1990) 169–179. https://doi.org/10.1007/BF01079045

[34] D.A. Garanin, Fokker-Planck and Landau-Lifshitz-Bloch equations for classical ferromagnets, Phys. Rev. B 55 (1997) 3050–3057. https://doi.org/10.1103/PhysRevB.55.3050

[35] C. Vogler, C. Abert, F. Bruckner, D. Suess, Landau-Lifshitz-Bloch equation for exchange-coupled grains, Phys. Rev. B 90 (2014) 214431. https://doi.org/10.1103/PhysRevB.90.214431

[36] A. Meo, W. Pantasri, W. Daeng-am, S.E. Rannala, S.I. Ruta, R.W. Chantrell, P. Chureemart, J. Chureemart, Magnetization dynamics of granular heat-assisted magnetic recording media by means of a multiscale model, Phys. Rev. B 102 (2020) 174419. https://doi.org/10.1103/PhysRevB.102.174419

[37] A. Truong, T. Maletzky, M. Dovek, B. Dieny, Quasi-equilibrium stoner-wohlfarth versus strongly out-of-equilibrium dynamics in HAMR, IEEE Trans. Magn. 58 (4) (2022) 1–9. https://doi.org/10.1109/TMAG.2021.3121624

[38] U. Atxitia, O. Chubykalo-Fesenko, N. Kazantseva, D. Hinzke, U. Nowak, R.W. Chantrell, Micromagnetic modeling of laser-induced magnetization dynamics using the Landau-Lifshitz-Bloch equation, Appl. Phys. Lett. 91 (23) (2007) 232507. https://doi.org/10.1063/1.2822807

[39] V. Raposo, E. Martínez, A. Hernández, M. Zazo, Micromagnetic modeling of all-optical switching, IEEE Trans. Magn. 55 (7) (2019) 1–6. https://doi.org/10.1109/TMAG.2018.2888902

[40] S. Moretti, V. Raposo, E. Martinez, L. Lopez-Diaz, Domain wall motion by localized temperature gradients, Phys. Rev. B 95 (2017) 64419. https://doi.org/10.1103/PhysRevB.95.064419

[41] N. Josten, B. Beckmann, R. Meckenstock, K.P. Skokov, H. Pazniak, T. Ouisse, N. Shkodich, A. Semisalova, O. Gutfleisch, M. Farle, U. Wiedwald, Temperature-dependent magnetocrystalline anisotropy of Fe_2AlB_2 single crystals, Phys. Rev. Mater. 9 (2025) 54405. https://doi.org/10.1103/PhysRevMaterials.9.054405

[42] A. Vansteenkiste, J. Leliaert, M. Dvornik, M. Helsen, F. Garcia-Sanchez, B.V. Waeyenberge, The design and verification of $MuMax^3$, AIP Adv. 4 (2014) 107133. https://doi.org/10.1063/1.4899186

[43] J.M.D. Coey, Magnetism and Magnetic Materials, Cambridge University Press, 2010. https://doi.org/10.1017/CBO9780511845000

[44] X. Tan, P. Chai, C.M. Thompson, M. Shatruk, Magnetocaloric effect in $AlFe_2B_2$: toward magnetic refrigerants from earth-abundant elements, J. Am. Chem. Soc. 135 (2013) 9553–9557. https://doi.org/10.1021/ja404107p

[45] L.H. Lewis, R. Barua, B. Lejeune, Developing magnetofunctionality: coupled structural and magnetic phase transition in $AlFe_2B_2$, J. Alloys Compd. 650 (2015) 482–488. https://doi.org/10.1016/j.jallcom.2015.07.255

[46] T.N. Lamichhane, L. Xiang, Q. Lin, T. Pandey, D.S. Parker, T.-H. Kim, L. Zhou, M.J. Kramer, S.L. Bud'ko, P.C. Canfield, Magnetic properties of single crystalline itinerant ferromagnet $AlFe_2B_2$, Phys. Rev. Mater. 2 (2018) 84408. https://doi.org/10.1103/PhysRevMaterials.2.084408

[47] B. Beckmann, T.A. El-Melegy, D. Koch, U. Wiedwald, M. Farle, F. Maccari, J. Snyder, K.P. Skokov, M.W. Barsoum, O. Gutfleisch, Reactive single-step hot-pressing and magnetocaloric performance of polycrystalline $Fe_2Al_{1.15-x}B_2Ge_xGa_x (x = 0, 0.05)$ MAB phases, J. Appl. Phys. 133 (2023) 173903. https://doi.org/10.1063/5.0143037

[48] N. Akulov, Zur quantentheorie der temperaturabhängigkeit der magnetisierungskurve, Zeitschrift für Physik 100 (1936) 197–202. https://doi.org/10.1007/BF01418601

[49] C. Zener, Classical theory of the temperature dependence of magnetic anisotropy energy, Phys. Rev. 96 (1954) 1335–1337. https://doi.org/10.1103/PhysRev.96.1335

[50] H.B. Callen, E. Callen, The present status of the temperature dependence of magnetocrystalline anisotropy, and the l(l+1)2 power law, J. Phys. Chem. Solids 27 (8) (1966) 1271–1285. https://doi.org/10.1016/0022-3697(66)90012-6

[51] R. Barua, B.T. Lejeune, L. Ke, G. Hadjipanayis, E.M. Levin, R.W. McCallum, M.J. Kramer, L.H. Lewis, Anisotropic magnetocaloric response in $AlFe_2B_2$, J. Alloys Compd. 745 (2018) 505–512. https://doi.org/10.1016/j.jallcom.2018.02.205

[52] H.B. Tran, H. Momida, Y.-i. Matsushita, K. Sato, Y. Makino, K. Shirai, T. Oguchi, Effect of magnetocrystalline anisotropy on magnetocaloric properties of an $AlFe_2B_2$ compound, Phys. Rev. B 105 (2022) 134402. https://doi.org/10.1103/PhysRevB.105.134402

[53] J. Leliaert, B.V. de Wiele, A. Vansteenkiste, L. Laurson, G. Durin, L. Dupré, B.V. Waeyenberge, Current-driven domain wall mobility in polycrystalline permalloy nanowires: a numerical study, J. Appl. Phys. 115 (2014) 233903. https://doi.org/10.1063/1.4883297

[54] V.K. Pecharsky, K.A. Gschneidner, Magnetocaloric effect from indirect measurements: magnetization and heat capacity, J. Appl. Phys. 86 (1999) 565–575. https://doi.org/10.1063/1.370767

[55] T. Diamantopoulos, L.M. Moreno-Ramírez, V. Franco, R. Bjørk, A fast 1D model of active magnetic regeneration with a compressible working fluid, Int. J. Refrig. 178 (2025) 359–366. https://doi.org/10.1016/j.ijrefrig.2025.07.005

[56] R. Caballero-Flores, V. Franco, A. Conde, L.F. Kiss, Influence of the demagnetizing field on the determination of the magnetocaloric effect from magnetization curves, J. Appl. Phys. 105 (2009) 07A919. https://doi.org/10.1063/1.3067463

[57] C. Romero-Muniz, J.J. Ipus, J.S. Blazquez, V. Franco, A. Conde, Influence of the demagnetizing factor on the magnetocaloric effect: critical scaling and numerical simulations, Appl. Phys. Lett. 104 (2014) 252405. https://doi.org/10.1063/1.4885110

[58] L.M. Moreno-Ramírez, J.J. Ipus, V. Franco, J.S. Blázquez, A. Conde, Analysis of magnetocaloric effect of ball milled amorphous alloys: demagnetizing factor and Curie temperature distribution, J. Alloys Compd. 622 (2015) 606–609. https://doi.org/10.1016/j.jallcom.2014.10.134

[59] Y. Liu, Z. Hu, C. Petrovic, Anisotropic magnetocaloric effect and critical behavior in $CrSbSe_3$, Phys. Rev. B 102 (2020) 14425. https://doi.org/10.1103/PhysRevB.102.014425

[60] M. Balli, S. Jandl, P. Fournier, M.M. Gospodinov, Anisotropy-enhanced giant reversible rotating magnetocaloric effect in $HoMn_2O_5$ single crystals, Appl. Phys. Lett. 104 (2014) 232402. https://doi.org/10.1063/1.4880818

[61] M. Fries, K.P. Skokov, D.Y. Karpenkov, V. Franco, S. Ener, O. Gutfleisch, The influence of magnetocrystalline anisotropy on the magnetocaloric effect: a case study on Co_2B, Appl. Phys. Lett. 109 (23) (2016) 232406. https://doi.org/10.1063/1.4971839